Journal of
Marine Science and Engineering

MDPI

Article

Information Capacity of Turbulent and Absorptive Underwater Wireless Link with Perfect Laguerre–Gaussian Beam and Pointing Errors

Yixin Zhang †, Qingze Yan †, Lin Yu and Yun Zhu *

School of Science, Jiangnan University, Wuxi 214122, China
* Correspondence: zhuyun1210@163.com
† These authors contributed equally to this work.

Abstract: The model of information capacity for underwater wireless optical communication (UWOC) links with pointing errors and the carrier of perfect Laguerre–Gaussian (PLG) beam in absorbed and weakly turbulent seawater is modeled. Using this model, the influence of channel parameters on the propagation of PLG beams is numerically analyzed. We show that the pointing error significantly reduces the performance of the optical transmission system. Large topological charge and radial orders are not conducive to high information capacity transmission. Additionally, the information capacity decreases with the increase in the spectral absorption coefficient of seawater. With higher transmission power, the transmission of an optical transmission system with high average capacity can be realized. The information capacity is affected by both signal wavelength and seawater absorption coefficient. That is, in the case of small seawater absorption and short message channel, the channel capacity loss of the link with long signal wavelength is smaller. In the case of long channels and strong seawater absorption, the influence of signal wavelength on the average capacity can be ignored. The information capacity of the communication link is the highest, which is composed of the carrier with the OAM topological charge, and the radial orders are both 1, and the wavelength is 410 nm.

Keywords: information capacity; pointing errors; perfect Laguerre–Gaussian; underwater turbulence; wireless optics communication

Citation: Zhang, Y.; Yan, Q.; Yu, L.; Zhu, Y. Information Capacity of Turbulent and Absorptive Underwater Wireless Link with Perfect Laguerre–Gaussian Beam and Pointing Errors. *J. Mar. Sci. Eng.* **2022**, *10*, 1957. https://doi.org/10.3390/jmse10121957

Academic Editors: Syed Agha Hassnain Mohsan, Mohammed H. Alsharif and Khaled Rabie

Received: 27 October 2022
Accepted: 6 December 2022
Published: 9 December 2022

1. Introduction

The underwater wireless optical communication (UWOC) system has the advantages of high anti-interference, high security, high information capacity (large bandwidth) and low cost, which has attracted increasing attention [1,2]. However, the performance of the UWOC system, especially the capacity of communication information, is severely restricted by the combined effects of seawater absorption, water flow [3], turbulence [4,5] and pointing error [6]. So far, there have been a lot of reports on the information capacity of UOWC links affected by turbulent seawater, such as as Gaussian beam (GB) with large wavelength and waist radius propagation in weak and unstable stratification ocean turbulence with large edge scale turbulence, including small pointing error and large information capacity [4]. The channel capacity of a UOWC link with GB in anisotropic strong oceanic turbulence is always greater than that of a UOWC link in isotropic strong oceanic turbulence for the same system parameters [7]. The average capacity of a UOWC link with partially coherent GB is slightly larger in clear ocean than in coastal ocean [8], and the converging Gaussian beam array can effectively reduce the scintillation caused by ocean turbulence in a UWOC link between misaligned sensors [9]. Cheng et al. [10] found that quasi-nondiffracting Bessel–Gauss (BG) beams have obvious advantages over Laguerre–Gaussian (LG) beams in reducing turbulence and improving the performance of OAM optical Communication Links in the weak turbulence region. In a weak UOWC link, large-capacity ocean optical

communication can be realized by using Bessel–Gaussian local wave (BGLV) [11] and Lommel–Gaussian local wave (LGLV) [12], and under certain parameters of a UOWC link, there exists the maximum effective waist. The channel capacity of the link can be increased by adopting a wider initial half-pulse width, smaller Bessel cone angle of BGLW and larger receiver aperture of the link [13]. Yang et al. [14] show that the transmission distance of OAM mode carried by POV [15,16] in four kinds of seawater is better than that of a Bessel–Gaussian beam [10]. For the link with coaxial double-position power Gaussian vortex carrier in weak turbulence, the link with high information capacity can be achieved by increasing the receiving aperture, reducing the diameter of the transmitting beam, adopting the long wavelength of the light source in the seawater window and multiple OAM channels [17]. In the link with strong oceanic turbulence and pointing error, the performance of the optics communication system can be improved significantly by a smaller rectangular QAM dimension in short distance, or a larger aperture diameter and the ratio of beam width to aperture radius [18]. There exists an optimizing half-beam width of perfect optical vortex (POV) link signal source of the UWOC link that is the function of the topological charge and transmission distance [19]. The UWOC link with perfect Laguerre–Gaussian (PLG) beam [20] can obtain high channel capacity by adopting low OAM topological charge and smaller aperture of transceiver system [21]. The channel capacity of free-space optical UWOC links is significantly enhanced with an aggregate transmission rate of 100 Gb/s by combining dual-wavelength wavelength division multiplexing and four-level pulse amplitude modulation [22]. Models for the outage probability and average channel capacity of the UWOC systems are proposed by the generalized Málaga fading model of weak-to-strong turbulent links [23,24]. The average symbol error probability and average channel capacity of the UWOC link with absorption, scattering and turbulence (modeled by Málaga distribution), and M-ary pulse position modulation (PPM), is under the constraints of the limited average power and peak power [25]. Compared with the LG beam and the BG beam, anti-diffraction and anti-attenuation of the random beam have a stronger ability to resist seawater turbulence and seawater absorption [26]. The existence of input-dependent noise severely degrades the channel capacity of the link with absorption and scattering losses [27]. Spatial diversity MIMO schemes can improve the UOWC link performance [28]. The POV beam could improve the capacity of the spatial-mode modulating, multiplexing and OAM-based UWOC link [29]. Choosing optimum beam source parameters is favorable to mitigate the influence of oceanic turbulence, and the partially coherent elegant LG beams are more affected by turbulence as compared with the fully coherent elegant LG beams [30].

As far as we know, the research on channel capacity affected by link pointing error in OAM underwater communication has not been reported in detail.

In this paper, the influence of absorption and weak turbulent seawater on the OAM mode of PLG beam propagation is studied from the point of view of the information capacity of the link when the link pointing error exists. In Section 2, the information capacity of the OAM communication link that has pointing errors is presented. The numerical simulations for demonstrating the relationships between the information capacity of the communication link and the parameters of the beam and turbulence are in Section 3. Finally, conclusions are given in Section 4.

2. Information Capacity of the Link with Perfect Laguerre–Gaussian Beam Carrier and Pointing Errors in Turbulent Seawater

2.1. Perfect Laguerre–Gauss Beam in Absorbing Turbulent Seawater

In the UWOC system model (Figure 1), the transmitter is composed of M-QAM modulator, light source and optical antenna. The receiver is made of an optical antenna, detector and demodulator.

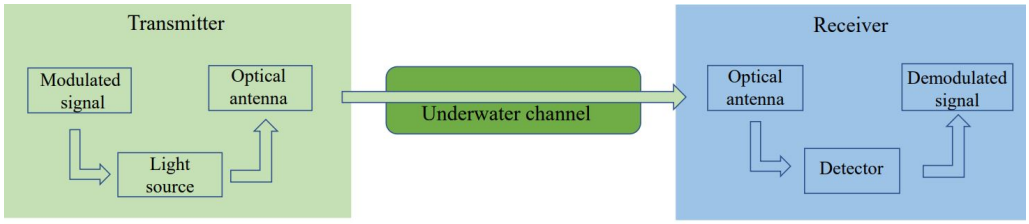

Figure 1. Schematic of underwater wireless optical communication system model.

In cylindrical polar coordinates (r, φ, z) , the normalized complex amplitude of the PLG beam at z plane from the source in absorbing seawater is represented by [19]

$$E_{m_0}(r,\varphi,z) = \frac{R_{m_0,p}(r,z)}{\sqrt{2\pi}} \exp(\mathrm{i}m_0\varphi + \mathrm{i}k_0 nz) \exp\left[-\mathrm{i}(2p+|m_0|+1)\delta_G - \frac{\alpha(\lambda)}{2}z\right], (m_0 \neq 0) \tag{1}$$

with the complex amplitude of the PLG beam $R_{m,,p}(r,z)$

$$\begin{aligned} R_{m_0,n}(r,z) = {} & \frac{1}{w(z)}\sqrt{\frac{4p!}{(p+|m_0|)!}}\left(\frac{\sqrt{2}r}{w(z)}\right)^{|m_0|} \mathrm{L}_p^{m_0}\left(\frac{2r^2}{w^2(z)}\right) \\ & \times \exp\left[-\left(\frac{1}{w^2(z)} - \frac{k_0 n}{2R(z)}\right)r^2\right] \exp\left(-\frac{\mathrm{i}k_0 n r^2}{2R(z)}\right), \end{aligned} \tag{2}$$

where r is the radial cylindrical coordinate, φ is the azimuthally angle, z is the propagation distance, $\mathrm{L}_p^{m_0}$represents the associated Laguerre polynomial, p is the radial orders and m_0 is the azimuthal orders, m_0 also notes the OAM topological charge of initial OAM modes, n is the refractive index of seawater and $\alpha(\lambda)$ represents the spectral absorption coefficient of seawater [20,22]; $w(z) = \frac{w_0}{2\sqrt{2p+(|m_0|+1)}}\sqrt{1+(z/z_R)^2}$ is the spot size of the PLG beam, w_0 is the waist of the Gaussian beam, $R(z) = z + z_{oR}^2/z$ is the radius of wave front curvature and $z_R = \frac{1}{2}k_0\sqrt{n^2 + \left(\frac{\lambda\alpha(\lambda)}{4\pi}\right)^2 w_{m_0 p}^2}$ is the Raleigh range of PLG beam in absorbing seawater and δ_G is the Gouy phase.

In Rytov approximation, we have the normalized complex amplitude of PLG vortex in turbulence absorptive seawater

$$E_m(r,\varphi,z) = E_{m_0}(r,\varphi,z)\exp[\psi(r,\varphi,z)], \tag{3}$$

where $\psi(r,\varphi,z)$ is the random complex phase factor caused by seawater turbulence.

2.2. Information Capacity of the OAM Channel without Pointing Errors

As the PLG beam propagates through the turbulent ocean, the beam is disturbed by refractive index fluctuations that alter the OAM mode of this beam. The fluctuation of the spectral absorption coefficient perturbs the complex amplitude of the wave so that it is no longer guaranteed to be in the original eigenstate of the OAM. The resulting wave is now written as a superposition of eigenstates [11]

$$E_m(r,\varphi,z) = \frac{1}{\sqrt{2\pi}}\sum_m b_p^m(r,z)\exp(\mathrm{i}m\varphi) \tag{4}$$

where m is the topological charge of the signal ($m = m_0$) and crosstalk ($m \neq m_0$) OAM modes, and $b_p^m(r,z)$ is the Fourier expansion coefficient, which is given by

$$b_p^m(z) = \frac{1}{\sqrt{2\pi}}\sum_{m-\infty}^{\infty}\int_0^{2\pi} E_{m_0}(r,\varphi,z)\exp[\psi(r,\varphi,z)]\exp(-\mathrm{i}m\varphi)\mathrm{d}\varphi. \tag{5}$$

Then, the probability distribution of the new OAM $l_z = m\hbar$ is obtained by summing the probabilities associated with that eigenvalue [20],

$$p_{m/m_0} = \sum_p \left\langle \left| b_p^m(r,z) \right|^2 \right\rangle, \tag{6}$$

where $\langle \cdot \rangle$ is the average of the seawater turbulence ensemble.

By Equations (5) and (6) and ref. [31], Equation (5) is expressed as [20]

$$\begin{aligned} p_{m/m_0} = {} & \frac{1}{2\pi} \iint E_{m_0}^*(r,\varphi',z) E_{m_0}(r,\varphi,z) \\ & \times \exp\left\{ -\left[1-\cos(\varphi-\varphi')\right] \frac{2r^2}{\rho_0^2} - im(\varphi-\varphi') \right\} \mathrm{d}\varphi' \mathrm{d}\varphi, \end{aligned} \tag{7}$$

where

$$\rho_o = \left\{ \frac{1}{3}\pi^2 k_0^2 \left[n^2 + \left(\frac{\lambda\alpha(\lambda)}{4\pi} \right)^2 \right] z \int_0^\infty \kappa^3 \Phi_n(\kappa) \mathrm{d}\kappa \right\}^{-1/2}, \tag{8}$$

In Equation (8), $\Phi_n(\kappa)$ is the power spectrum of the fluctuations of the refractive index of seawater in stable stratification and anisotropic turbulence that is given by [4,11]

$$\begin{aligned} \Phi_n(\kappa,\zeta) = {} & \frac{0.033 C_{\epsilon\chi_T}^2 \zeta^2 \kappa^{-11/3} \left[1 + 4.6(\kappa\eta)^{2/3} \right]}{(1-\varpi)^2 \left(\kappa^2 + \kappa_0^2\right)^{11/6}} \\ & \times \left[\varpi^2 \exp\left(-\kappa^2/\kappa_T^2\right) + \exp\left(-\kappa^2/\kappa_S^2\right) - 2\varpi \exp\left(-\kappa^2/\kappa_{TS}^2\right) \right], \quad 0 < \kappa < \infty, \end{aligned} \tag{9}$$

where κ represents the scalar spatial wave number of refractive index of seawater turbulence, ζ is the turbulence anisotropy index, $C_{\varepsilon\chi_T}^2 = 0.809 \times 10^{-7} \varepsilon^{-1/3} \chi_T \overline{\omega}^{-2} (1-\overline{\omega})^2 \left(\mathrm{K}^2/\mathrm{m}^{2/3} \right)$ is the structural constant of oceanic turbulence, ϵ is the rate of dissipation of kinetic energy per unit mass of fluid, ϵ is in the range $\left[10^{-10}, 10^{-1}\right] \mathrm{m}^2/\mathrm{s}^3$, χ_T is the dissipation rate of the mean-squared temperature ranging from $10^{-10} \mathrm{K}^2/\mathrm{s}$ to $10^{-2} \mathrm{K}^2/\mathrm{s}$ and $\overline{\omega}$ represents the ratio of temperature and salinity contributions to the refractive index fluctuations and varies in the interval $(-5, 0)$ in seawater. $\kappa_0 = 2\pi/L_0$, $\kappa_T = R_T/\eta$, $\kappa_S = R_S/\eta$, $\kappa_{TS} = R_{TS}/\eta$, η is turbulent inner scale, L_0 is the outer scale of turbulence, $R_j = \sqrt{3}\left[W_j - 1/3 + 1/\left(9W_j\right)\right]^{3/2}/Q^{-3/2} (j = T, S, TS)$, $W_j = \left\{ \left[\frac{\mathrm{Pr}_j^2 Q^4}{(6\beta)^2} - \frac{\mathrm{Pr}_j Q^2}{81\beta} \right]^{1/2} - \left[\frac{1}{27} - \frac{\mathrm{Pr}_j Q^2}{6\beta} \right] \right\}^{1/3}$ and Q is the nondimensional constant; Pr_T and Pr_S, respectively, represent the Prandtl number of the temperature and salinity, $\mathrm{Pr}_{TS} = 2\,\mathrm{Pr}_T\,\mathrm{Pr}_S/(\mathrm{Pr}_T + \mathrm{Pr}_S)$.

The transverse spatial coherence radius of the spherical wave represented by Equations (8) and (9) is given by the following formula [20]

$$\begin{aligned} \rho_o = {} & \left\{ \frac{2.144\left[n^2 + \left(\frac{\lambda\alpha(\lambda)}{4\pi}\right)^2\right] C_{\varepsilon\chi_T}^2 z}{\lambda^2 \zeta^2 (1-\varpi)^2} \kappa_0^{1/3} \left[\varpi^2 \mathrm{U}\left(2; \frac{7}{6}; \frac{\kappa_0^2}{\kappa_T^2}\right) + \mathrm{U}\left(2; \frac{7}{6}; \frac{\kappa_0^2}{\kappa_S^2}\right) \right. \right. \\ & \left. -2\varpi \mathrm{U}\left(2; \frac{7}{6}; \frac{\kappa_0^2}{\kappa_{TS}^2}\right) \right] + 9.862 l_0^{2/3} \kappa_0 \Gamma\left(\frac{7}{3}\right) \frac{\left[n^2 + \left(\frac{\lambda\alpha(\lambda)}{4\pi}\right)^2 \right] C_{\varepsilon\chi_T}^2 z}{\lambda^2 (1-\varpi)^2} \\ & \left. \times \left[\varpi^2 \mathrm{U}\left(\frac{7}{3}; \frac{3}{2}; \frac{\kappa_0^2}{\kappa_T^2}\right) + \mathrm{U}\left(\frac{7}{3}; \frac{3}{2}; \frac{\kappa_0^2}{\kappa_S^2}\right) - 2\varpi \mathrm{U}\left(\frac{7}{3}; \frac{3}{2}; \frac{\kappa_0^2}{\kappa_{TS}^2}\right) \right] \right\} \Bigg\}^{-1/2}, \end{aligned} \tag{10}$$

where $\Gamma(\cdot)$ is gamma function, and $\mathrm{U}(\cdot)$ is the confluent hypergeometric function of the second kind.

Substitute Equations (1) and (2) into Equation (7), we obtain

$$p_{m/m_0} = \frac{4p!\exp[-\alpha(\lambda)z]}{(2\pi)^2 w(z)^2 (p+|m_0|)!}\left(\frac{\sqrt{2}r}{w(z)}\right)^{|2m_0|}\exp\left[-2\left(\frac{1}{w^2(z)}-\frac{k_0 n}{2R(z)}+\frac{1}{\rho_0^2}\right)r^2\right] \times \left|\mathrm{L}_p^{m_0}\left(\frac{2r^2}{w^2(z)}\right)\right|^2\left\{\int_0^{2\pi}\int_0^{2\pi}\exp\left[2\cos(\varphi-\varphi')\frac{r^2}{\rho_0^2}-\mathrm{i}(m-m_0)(\varphi-\varphi')\right]\mathrm{d}\varphi'\mathrm{d}\varphi\right\}. \tag{11}$$

By the integral relationship of Equation (BI 277) in ref. [32], Equation (11) can be represented as

$$p_{m/m_0} = \frac{4\pi p!\exp[-\alpha(\lambda)z]}{w^2(z)(p+|m_0|)!}\left(\frac{2r^2}{w^2(z)}\right)^{|m_0|}\exp\left(-\frac{r^2}{w_{eff}^2}\right)\mathrm{I}_{m-m_0}\left(\frac{2r^2}{\rho_o^2}\right)\left|\mathrm{L}_p^{m_0}\left(\frac{2r^2}{w^2(z)}\right)\right|^2, \tag{12}$$

where $w_{eff} = \left(\frac{4\sqrt{2p+(|m_0|+1)}}{\left(w_0\sqrt{1+(z/z_R)^2}\right)^2}+\frac{2}{\rho_o^2}-\frac{\alpha(\lambda)z}{2R(z)}\right)^{-1/2}$, where $\mathrm{I}_m(\cdot)$ is the Bessel function of second kind with m order.

The probability distribution for P_{m/m_0} of the OAM mode can be expressed as

$$p(P_{m/m_0}) = \frac{P_{m/m_0}}{\sum_{q=-\infty}^{\infty} P_{q/q_0}}, \tag{13}$$

and

$$P_{m/m_0} = 2\pi\int_0^{D/2} p_{m/m_0} r\,\mathrm{d}r, \tag{14}$$

where D is diametet of receiver.

2.3. Information Capacity and OAM Signal Detection Probability for Link with Pointing Errors

In order to obtain a theoretical model of the information capacity of underwater optical communication links, we first derive the theoretical relation of bit error rate of communication link with pointing error. When a Gaussian beam of beam width w_0 propagates from the transmitter to the detector plane z, the fraction of power collected by the receiver can be approximated as [33]

$$f(\sigma_s) \approx |\operatorname{erf}(v)|^2\exp\left(-\frac{2\sigma_s^2}{w_{eq}^2(z)}\right), \quad w_{eff}(z) > 3\frac{w_0}{\sqrt{2p+(|m_0|+1)}}, \tag{15}$$

where $w_{eff}(z)$ is the beam width of Gaussian beam at detector plane z, σ_s is the radial displacement between the centers of the beam and detector, $v = \sqrt{\frac{\pi w_0^2}{4w_{eff(z)}^2(z)(2p+(|m_0+1))}}$ is the ratio between the aperture radius w_0 and the beam width $w_{eff}(z)$, $\operatorname{erf}(x) = \frac{2}{\sqrt{\pi}}\int_0^x \exp(-t^2)\mathrm{d}t$ is the error function and $w_{eff}(z)$ is the equivalent beam width defined by $w_{eq}^2(z) = w_{eff}^2(z)\frac{\sqrt{\pi}|\operatorname{erf}(v)|^2}{2v\exp(-v^2)}$.

The probability distribution for $f[f(\sigma_s)]$ can be expressed as [33]

$$f[f(\sigma_s)] = \frac{\gamma^2}{|\operatorname{erf}(v)|^{2\gamma^2}} f(\sigma_s)^{\gamma^2-1}. \tag{16}$$

In Equation (16), $\gamma = w_{eq}(z)/2\sigma_s$ and σ_s is the standard deviation of transverse displacement of link pointing (or pointing error) at the receiver.

The intensity of $P_{m,m_0,p} = P_{m/m_0} f(\sigma_s)$ can be expressed as

$$p_{m,m_0,p} = \int_{P_{m/m_0} f(\sigma_s)/|\operatorname{erf}(v)|^2}^{\infty} f\left(P/P_{m/m_0}\right) p\left(P_{m/m_0}\right) \mathrm{d}P_{m/m_0}, \tag{17}$$

where

$$f\left(P/P_{m/m_0}\right) = \frac{\gamma^2}{P_{m/m_0}|\operatorname{erf}(v)|^{2\gamma^2}} \left(\frac{P_{m,m_0,p}}{P_{m/m_0}}\right)^{\gamma^2-1}. \tag{18}$$

Substitute Equation (18) into Equation (17), and rewrite Equation (18) as

$$\begin{aligned} p_{m,m_0,p} &= \frac{\gamma^2}{|\operatorname{erf}(v)|^{2\gamma^2} \sum_{q=-\infty}^{\infty} P_{q/q_0}} \int_{P_{m/m_0} f(\sigma_s)/|\operatorname{erf}(v)^2|}^{\infty} {P_{m/m_0}}^{1-\gamma^2} \, \mathrm{d}P_{m/m_0} \\ &= \frac{\gamma^2 f(\sigma_s)}{(\gamma^2-2)|\operatorname{erf}(v)|^4} p\left(P_{m/m_0}\right). \end{aligned} \tag{19}$$

For $m \neq m_0$, $p_{mm_0,p} = p_{m\neq m_0,p}$ is the crosstalk probability of the OAM mode, which describes the probability of the photon migrating from the OAM signal mode to the new OAM mode, and $p_{mm_0,p} = p_{m=m_0,p}$ is the signal probability of the OAM mode.

When the transmit power is large sufficient, the signal-to- noise- crosstalk ratio (SNCR) of the OAM channel is approximately [34]

$$SNCR_{m,m_0} = \frac{p_{m=m_0,p}}{\sum_{m=-\infty}^{\infty} p_{m\neq m_0,p} + \frac{N_0}{P_{TX}}}, \tag{20}$$

where $\sum_{m=-\infty}^{\infty} p_{m\neq m_0,p}$ is OAM crosstalk noise. N_0/P_{TX} represents the ratio of channel noise and transmit power.

For signal modulation of M-QAM, based on SNCR, the symbol error probabilities of the M-QAM OAM channel are, respectively, expressed as [1,34]

$$\begin{aligned} BER_{M-QAM} = {} & \frac{2}{\log_2 M}\left(1-\frac{1}{\sqrt{M}}\right) \operatorname{erfc}\sqrt{\frac{3\log_2 M}{2(M-1)} SNCR_{m,m_0}} \\ & \times \left[1-\frac{1}{2}\left(1-\frac{1}{\sqrt{M}}\right) \operatorname{effc}\sqrt{\frac{3\log_2 M}{2(M-1)} SNCR_{m,m_0}}\right]. \end{aligned} \tag{21}$$

The information capacity of the OAM channel with signal modulation of M-QAM can be described by the following formula

$$\begin{aligned} C_{M-QAM} = {} & \log_2 N + \left(1-BER_{M-QAM}\right)\log_2\left(1-BER_{M-QAM}\right) \\ & + BER_{M-QAM}\log_2 \frac{BER_{M-QAM}}{N-1}, \end{aligned} \tag{22}$$

where $N = -m, -m+1, \cdots, 0, \cdots m-1, m$.

3. Numeric Analysis

In this section, we analyze the information capacity of the UWOC link with PLG beam in turbulence and absorbable seawater through numerical simulation. Among other things, in the numerical analysis below, we select the parameters listed in Table 1 from the available experiments [12,20,35].

Table 1. Major system parameters.

Symbol	Parameters	Value
Pr_T	Prandtl number of the temperature	0.72
Pr_S	Prandtl number of the salinity	700
Q	Nondimensional constant	2.5
ε	Rate of dissipation of kinetic energy per unit mass of fluid	10^{-3} $\mathrm{m}^2/\mathrm{s}^3$
χ_T	Dissipation rate of the mean-squared temperature	10^{-7} K^2/s
$\overline{\omega}$	Ratio of temperature and salinity	-4.5
k_0	Wave number	$2\pi/\lambda$
η	Inner scale	0.001 m
L_0	Outer scale	10 m
m_0	OAM topological charge	1
p	Radial order	0
D	Receiver diameter	0.05 m
w_0	Half-beam width	0.012 m
λ	Wavelength	410 nm
z	Propagation distance	100 m
M	Modulation order	256
σ_s	Pointing errors	0.03 m
ζ	Anisotropy index	2

First of all, to compare whether the scheme using PLG vortex as carrier is more conducive to reducing the link information capacity loss caused by absorbing turbulent seawater than the scheme using POV as carrier in UWOC, the numerical curves of the channel capacity of the PLG carrier and POV carrier links with the evolution of turbulence strength and transmission distance are presented in Figure 2 and Figure 3, respectively.

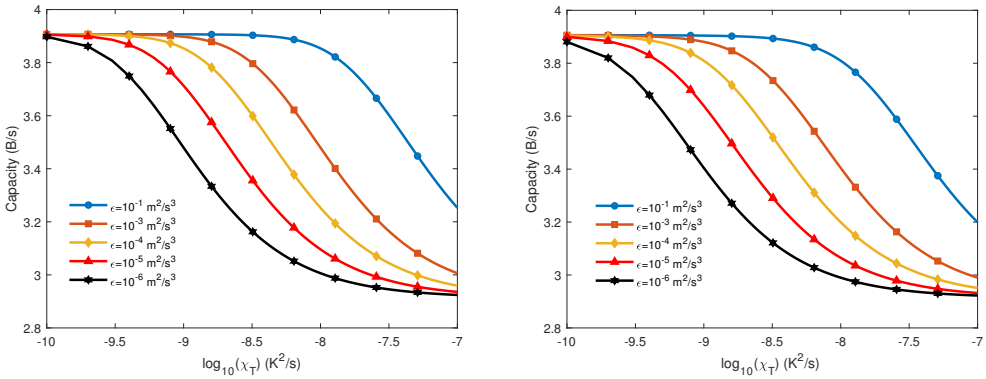

(**a**) PLG vortex (**b**) POV vortex

Figure 2. Information capacity of OAM channels with the carriers of PLG vortex and POV vortex versus dissipation rate of the mean-squared temperature χ_T and dissipation rate of kinetic energy per unit mass of fluid ε.

The relation diagram with the dissipation rate of the mean-squared temperature χ_T and the dissipation rate of kinetic energy per unit mass ϵ of fluid as independent variables and information capacity as function is drawn in Figure 2. Figure 2 reveals that the information capacity increases with the increase in ϵ or the decrease in χ_T, which can be explained since the larger ϵ or the smaller χ_T mean a weaker seawater turbulence, and PLG forms a smaller wavefront distortion. Comparing Figure 2a,b, we can see that the loss of the channel capacity of the PLG carrier link is less than that of the PLG carrier link under the same turbulence conditions and the same other link parameters (see Table 2).

Figure 3 shows the influence of the signal wavelength, propagation distance and seawater absorption on the propagation performance of the OAM mode. In the case of small seawater absorption and short message channel, the information capacity loss of the link with long signal wavelength is smaller. This result comes from the fact that the longer the signal wavelength is, the smaller the signal scintillation generated by turbulence is [30]. However, in the case of a long channel and strong seawater absorption, the influence of

signal wavelength on the information capacity can be ignored. Additionally, the greater the seawater absorption, the more serious the loss of link channel capacity. Comparing Figure 3a,b, we can see that similar to Figure 2, the loss of channel capacity of the PLG carrier link is less than that of the PLG carrier link at the same transmission distance and the same other link parameters. The specific comparison values are shown in Table 2.

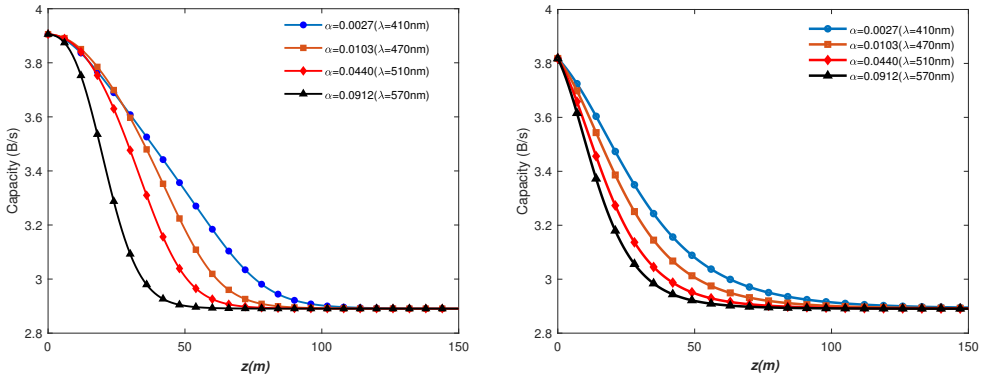

(**a**) PLG vortex (**b**) POV vortex

Figure 3. Information capacity of OAM channels with the carriers of PLG vortex and POV vortex versus signal wavelength and propagation distance.

Table 2. Performance comparison between PLG system and POV system.

Parameters	PLG Vortex Information Capacity (B/s)	POV Vortex Information Capacity (B/s)
$\varepsilon = 10^{-1}\,\mathrm{m}^2/\mathrm{s}^3$, $\chi_T = 10^{-9}\,\mathrm{K}^2/\mathrm{s}$	3.907	3.907
$\varepsilon = 10^{-1}\,\mathrm{m}^2/\mathrm{s}^3$, $\chi_T = 10^{-8}\,\mathrm{K}^2/\mathrm{s}$	3.854	3.809
$\varepsilon = 10^{-1}\,\mathrm{m}^2/\mathrm{s}^3$, $\chi_T = 10^{-7}\,\mathrm{K}^2/\mathrm{s}$	3.253	3.200
$\varepsilon = 10^{-3}\,\mathrm{m}^2/\mathrm{s}^3$, $\chi_T = 10^{-9}\,\mathrm{K}^2/\mathrm{s}$	3.899	3.881
$\varepsilon = 10^{-3}\,\mathrm{m}^2/\mathrm{s}^3$, $\chi_T = 10^{-8}\,\mathrm{K}^2/\mathrm{s}$	3.479	3.403
$\varepsilon = 10^{-3}\,\mathrm{m}^2/\mathrm{s}^3$, $\chi_T = 10^{-7}\,\mathrm{K}^2/\mathrm{s}$	3.006	2.98
$z = 50\,\mathrm{m}$, $\alpha = 0.0027$	3.386	3.078
$z = 50\,\mathrm{m}$, $\alpha = 0.0440$	3.192	3.009

Figure 4 shows the relationship between the information capacity and transverse pointing errors for different signal wavelength. The results of Figure 4 indicate that with the increase in pointing errors σ_s , the information capacity of links decreases. The reason is that when the pointing errors increases, part of the signal deviates from the receiver and cannot be received, which leads to a decrease in information capacity. In addition, as the pointing error increases, the average capacity of long-wavelength signals decays faster than that of short-wavelength signals, indicating that long-wavelength signals are more susceptible to pointing error. This is because seawater absorbs the signal corresponding to long wavelengths strongly, making the signal reaching the receiver weaker, resulting in long-wavelength signals being more susceptible to pointing errors.

Figure 5 indicates the information capacity of OAM link as a function of the inner and outer scales of seawater turbulence. Figure 5 shows that the information capacity increases as the inner scale of the turbulence increases and decreases as the outer scale of the turbulence decreases. This is due to the fact that as the inner scale of the turbulence increases, the uniform area in the seawater increases, and the wavefront distortion of the OAM signal mode through the channel decreases, that is, the transmission of the OAM signal mode increases. On the other hand, the transmission channel with large outer turbulence scale will cause large random deflections of the light rays, which results in large random optical path differences between the sub-beams of the OAM mode and, eventually, will lead to large wavefront distortion of the OAM mode and produce large OAM crosstalk.

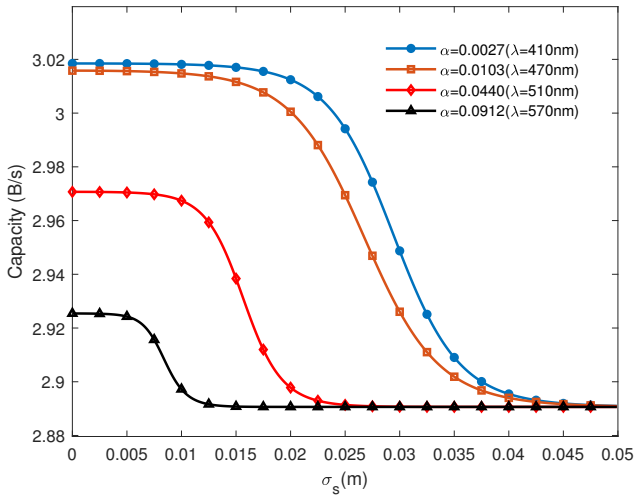

Figure 4. Information capacity of OAM channels versus the inner scale η for the outer scale L_0 .

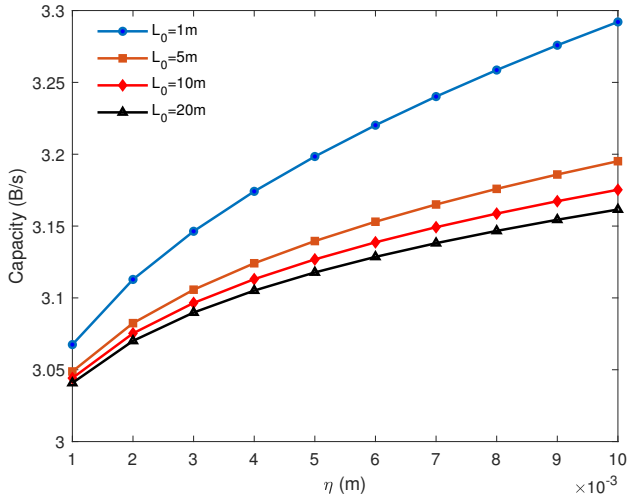

Figure 5. Information capacity of OAM channels versus receiving diameter D and pointing errors.

Figure 6 indicates the relationship between the information capacity and pointing errors for the different receiver diameter D. Figure 6 shows that as the pointing errors is small, the link with smaller receiver aperture has a larger information capacity. The reasons for the results are: (1) The average radius of the OAM modes of each order that make up the PLG beam increases with the increase in the absolute value of the topological charge of the OAM mode. (2) The topological load of the signal OAM mode in Figure 6 is $|1|$, and the topological charge of the crosstalk mode is $> |1|$. (3) The average channel capacity is calculated as the information capacity per unit area in the receiving plane. However, as the pointing error is large, the link with larger receiver aperture has a larger average capacity. Furthermore, when the pointing error is further increased to a sufficient size, the link channel capacity decreases slowly and tends to be independent of the receive aperture size. The physical basis of this result is as follows: when the receiving aperture of the communication system is larger, the background noise outside the signal it collects is larger.

In Figure 7, we show the information capacity of the OAM link as the function of half-beam width for different pointing errors under the condition that the receiver aperture is given. It can be seen from Figure 7 that there exists optimal $\tilde{w}_{\mathrm{opt}}(z)$ with maximum information capacity as the function of the channel length. In addition, the information capacity

and maximum information capacity decrease with the increase in σ_s. Additionally, the optimal $\tilde{w}_{\text{opt}}(z)$ increases as with an increase in σ_s.

In Figure 8, the relationship between the ratio of temperature and salinity ϖ and the information capacity of the link under different turbulence anisotropy index is studied. From Figure 8, it can be clearly found that, similar to communication links with other light beams as carriers [10,12–14], with the increase in ϖ , the information capacity decreases because of the increase in ϖ. In addition, with the increase in turbulence anisotropy index, the information capacity increases. This shows the larger anisotropic index ζ is conducive to the transiting of signal vortex modes.

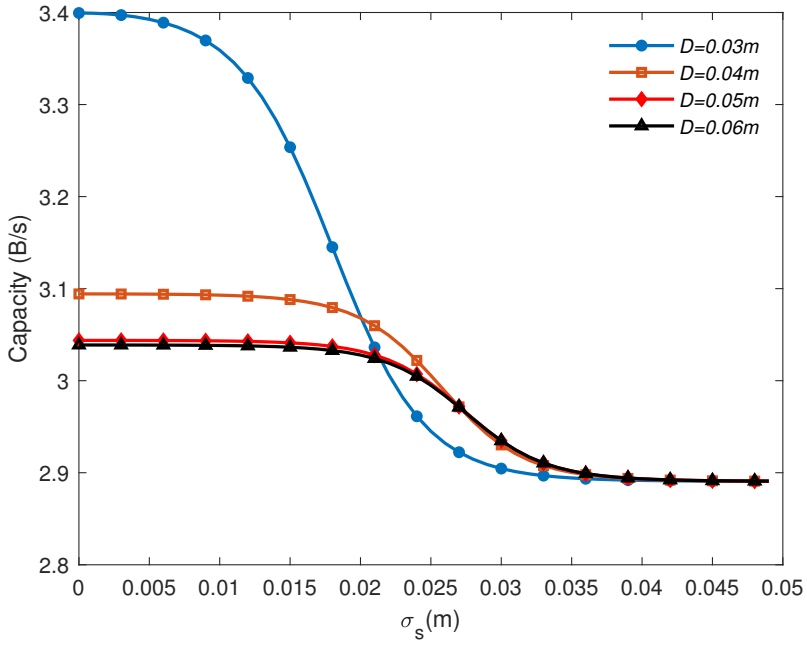

Figure 6. Information capacity of OAM channels versus the half-beam width and pointing errors.

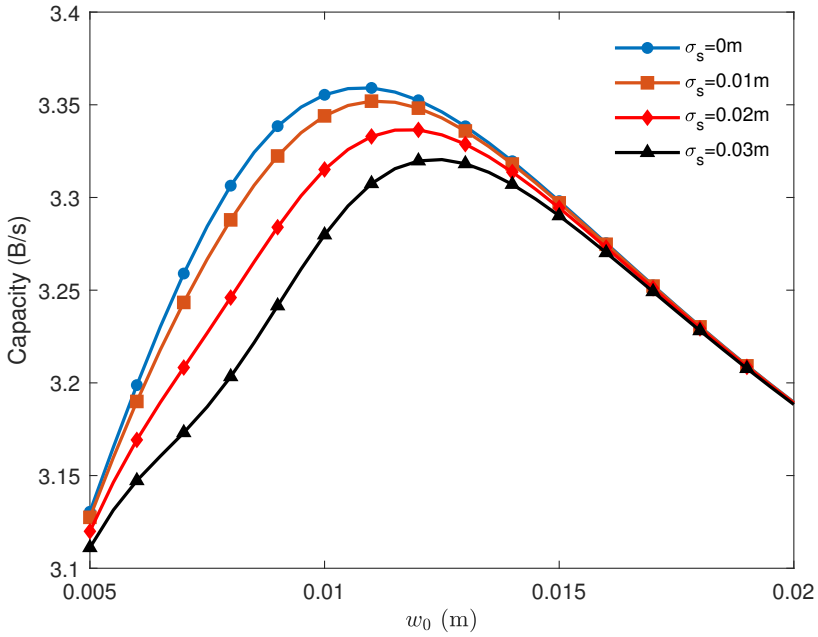

Figure 7. Information capacity of OAM channels versus the ratio of temperature and salinity ϖ and turbulence anisotropy index.

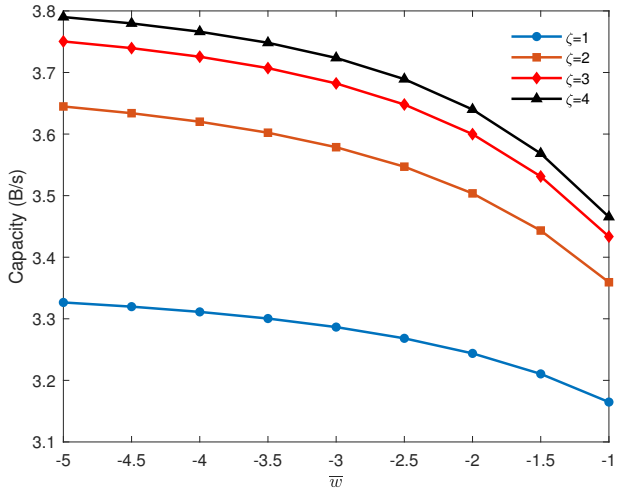

Figure 8. Information capacity of OAM channels versus dissipation rate of the mean-squared temperature χ_T and dissipation rate of kinetic energy per unit mass of fluid ϵ .

Figure 9 shows the relationship between information capacity and topological charge number m_0 with the different radial order of PLGs p. As can be seen from Figure 9, with the increase in the radial order of PLGs p , the information capacity decreases. This is because the increase in p leads to more rings at the receiver, which disperses the signal strength and leads to the decrease in the received information. In addition, with the increase in m_0 , the information capacity also decreases. This is because when the OAM topological charge m_0 increases, the dark spots of light intensity in the receiving plane are large, leading to the decrease in the amount of information detected by the receiver at the receiver.

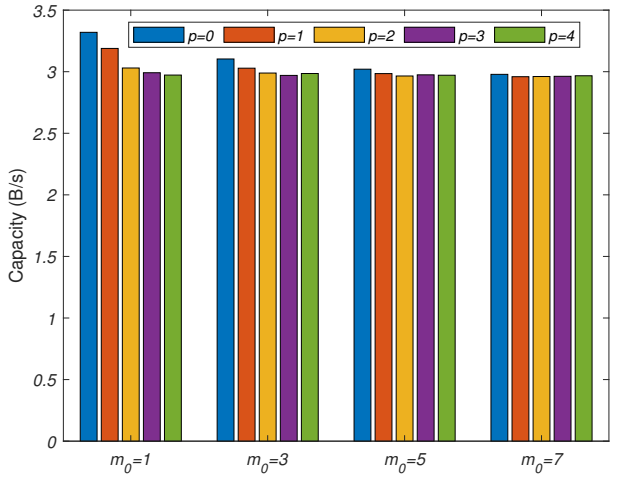

Figure 9. Information capacity of OAM channels versus topological charge number m_0 and PLGs p.

Figure 10 shows the influence of the ratio of noise to system power P_{TX}/N_0 on the information capacity of the link. In Figure 10, with the increase in the ratio of noise to system power P_{TX}/N_0, the information capacity increases. Because P_{TX}/N_0 increases, which means N_0 decreases, or P_{TX} increases, when N_0 decreases, and system noise decreases, it leads to a decrease in interference with the signal. Similarly, when P_{TX} increases, the power of the system increases, and the signal is not susceptible to noise. In addition, with the increase kin channel number N, the average capacity also increases.

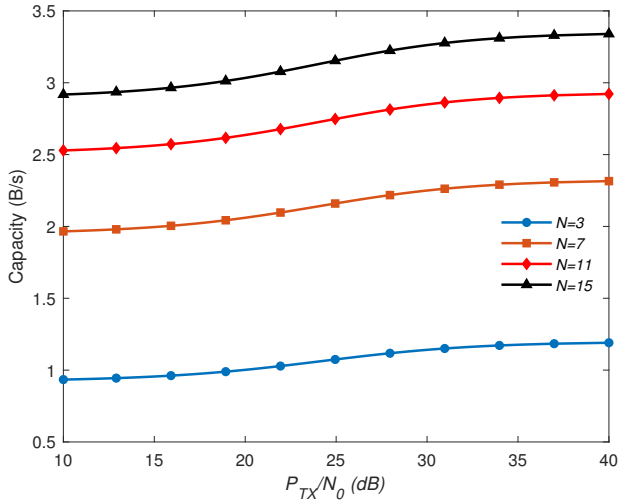

Figure 10. Information capacity of OAM channels versus the ratio of noise to system power P_{TX}/N_0 and channel number N.

4. Conclusions

This paper focuses on the influence of the anisotropy of ocean turbulence, and the pointing error of the system on the information capacity of an optical communication link with PLG vortex beam as the carrier in the channel of turbulence absorbing seawater does not take into account the scattering of seawater under 256-QAM modulation. The information capacity of the optics communication link is derived based on the Rytov approximation for weak turbulence. By comparing the loss of channel capacity of PLG and POV carrier links under the same conditions, which carrier is more suitable to be used as the optical communication carrier in the absorbing turbulent sea channel is studied. We came to the important conclusion that the link composed of the PLG carrier is better than that composed of the POV carrier. In low-absorption turbulent seawater with a short communication link, the transmission signal with longer wavelength is beneficial to reduce the loss of information capacity of communication links. The information capacity decreases with the increase in transmission distance, pointing errors, dissipation rate of the mean-squared temperature, topological charges m_0 of OAM mode, PLG's radial order and the outer scale of seawater turbulence, The information capacity of the OAM channel increases with the increase in the rate of dissipation of kinetic energy per unit mass of fluid, channel numbers, anisotropic index of turbulence, SNR of transceiver system and inner scale of seawater turbulence. Moreover, the long wavelength (or high absorption coefficient) signal and large receiver aperture are more susceptible to the pointing errors.

Author Contributions: Conceptualization, Y.Z. (Yixin Zhang); methodology, Y.Z. (Yixin Zhang); software, Q.Y.; validation, Y.Z. (Yixin Zhang), Q.Y. and Y.Z. (Yun Zhu); formal analysis, Q.Y.; investigation, Q.Y.; resources, Y.Z. (Yixin Zhang); data curation, Q.Y.; writing—original draft preparation, Y.Z. (Yun Zhu) and L.Y.; writing—review and editing, Y.Z. (Yixin Zhang); visualization, Q.Y.; supervision, Y.Z. (Yixin Zhang) and Y.Z. (Yun Zhu); project administration, Y.Z. (Yixin Zhang) and Y.Z. (Yun Zhu); funding acquisition, Y.Z. (Yixin Zhang) and Y.Z. (Lin Yu). All authors have read and agreed to the published version of the manuscript.

Funding: This research was funded by the National Natural Science Foundation of China (61871202, 11904136).

Data Availability Statement: Not applicable.

Conflicts of Interest: The authors declare no conflict of interest.

References

1. Wang, Z.; Zhang, P.; Qiao, C.; Lu, L.; Fan, C.; Ji, X. Scintillation index of Gaussian waves in weak turbulent ocean. *Opt. Commun.* **2016**, *380*, 79–86. [CrossRef]
2. Chen, Y.; Zhang, L.; Ling, Y. New approach for designing an underwater free-space optical communication system. *Front. Mar. Sci.* **2022**, *9*, 971559. [CrossRef]
3. Ijeh, I.C.; Khalighi, M.A.; Elamassie, M.; Hranilovic, S.; Uysal, M. Outage probability analysis of a vertical underwater wireless optical link subject to oceanic turbulence and pointing errors. *J. Opt. Commun. Netw.* **2022**, *14*, 439–453. [CrossRef]
4. Li, Y.; Zhang, Y.; Zhu, Y. Capacity of underwater wireless optical links with pointing errors. *Opt. Commun.* **2019**, *446*, 16–22. [CrossRef]
5. Yang, H.; Zhang, Y.; Zhao, G.; Yu, L.; Hu, L. Wander and spread of a perfect Laguerre–Gauss beam under turbulent absorbent seawater. *Appl. Opt.* **2022**, *61*, 4549–4557. [CrossRef]
6. Weng, Y.; Matsuda, T.; Sekimori, Y.; Pajarinen, J.; Peters, J.; Maki, T. Pointing error control of underwater wireless optical communication on mobile platform. *IEEE Photon. Technol. Lett.* **2022**, *34*, 699–702. [CrossRef]
7. Muhsin, C.G. Average capacity analysis of underwater optical wireless communication links over anisotropic strong oceanic turbulence channels. *J. Opt. Soc. Am. A* **2019**, *36*, 2040–2047.
8. Zou, Z.; Wang, P.; Chen, C.; Li, A.; Tian, H.; Guo, L. Average capacity of a UWOC system with partially coherent Gaussian beams propagating in weak oceanic turbulence. *J. Opt. Soc. Am. A* **2019**, *36*, 1463–1474. [CrossRef]
9. Cui, Z.; Yue, P.; Xiang, P.; Li, J. Effect of convergent beam array on reducing scintillation in underwater wireless optical communications with pointing errors. *Opt. Express* **2021**, *29*, 9846–9860. [CrossRef]
10. Cheng, M.; Guo, L.; Li, J.; Zhang, Y. Channel capacity of the OAM based free-space optical communication links with Bessel–Gauss beams in turbulent ocean. *IEEE Photonics J.* **2016**, *8*, 7901411. [CrossRef]
11. Yang, D.; Zhang, Y.; Shi, H. Capacity of turbulent ocean links with carrier Bessel–Gaussian localized vortex waves. *Appl. Opt.* **2019**, *58*, 9484–9490. [CrossRef]
12. Wang, S.; Yang, D.; Zhu, Y.; Zhang, Y. Capacity analysis of oceanic channels with localized Lommel–Gaussian vortex beams. *Appl. Opt.* **2021**, *60*, 4135–4142. [CrossRef]
13. Deng, S.; Yang, D.; Zhang, Y. Capacity of communication link with carrier of vortex localized wave in absorptive turbulent seawater. *Waves Random Complex Media* **2020**, *32*, 2124–2137. [CrossRef]
14. Yang, H.; Yan, Q.; Zhang, Y.; Hu, L. Received probability of perfect optical vortex in absorbent and weak turbulent seawater Links. *Appl. Opt.* **2021**, *60*, 10772–10779. [CrossRef]
15. Ostrovsky, A.S.; Ricrenstorff-Parrao, C.; Arrizón, V. Generation of the 'perfect' optical vortex using a liquid-crystal spatial light modulator. *Opt. Lett.* **2013**, *38*, 534–536. [CrossRef]
16. Jiang, X.; Tian, Y.; Sun, M.; Li, Z.; Zhang, D.; Cao, K.; Shi, Q.; Zhu, L. Perfect Optical Vortex to Produce Controllable Spot Array. *Front. Phys.* **2022**, *10*, 879689. [CrossRef]
17. Yan, Q.; Zhu, Y.; Zhang, Y. Capacity of the weakly absorbent turbulent ocean channel with the coaxial double-position power Gaussian vortex. *J. Mar. Sci. Eng.* **2021**, *9*, 1117. [CrossRef]
18. Fu, Y.; Duan, Q.; Huang, C.; Du, Y.; Zhou, L. Average BER performance of rectangular QAM-UWOC over strong oceanic turbulence channels with pointing error. *Opt. Commun.* **2020**, *476*, 126362. [CrossRef]
19. Mendoza-Hernandez, J.; Hidalgo-Aguirre, M.; Ladino, A.I.; Lopez-Mago, D. Perfect Laguerre–Gauss beams. *Opt. Lett.* **2020**, *45*, 5197–5200. [CrossRef]
20. Yang, H.; Yan, Q.; Wang, P.; Hu, L.; Zhang, Y. Bit-error rate and average capacity of an absorbent and turbulent underwater wireless communication link with perfect Laguerre-Gauss beam. *Opt. Express* **2022**, *30*, 9050–9064. [CrossRef]
21. Yan, Q.; Zhang, Y.; Yu, L.; Zhu, Y. Absorptive turbulent seawater and parameter optimization of perfect optical vortex for optical communication. *J. Mar. Sci. Eng.* **2022**, *10*, 1256. [CrossRef]
22. Li, C.; Huang, X.; Lu, H.; Huang, Y.; Huang, Q.; Tu, S. A WDM PAM4 FSO–UWOC integrated system with a channel capacity of 100 Gb/s. *J. Light. Technol.* **2020**, *38*, 1766–1776. [CrossRef]
23. Xu, G.; Song, Z.; Zhang, Q. Outage probability and channel capacity of an optical spherical wave propagating through anisotropic weak-to-strong oceanic turbulence with Málaga distribution. *J. Opt. Soc. Am. A* **2020**, *37*, 1622–1629. [CrossRef] [PubMed]
24. Xu, G.; Lai, J. Average capacity analysis of the underwater optical plane wave over anisotropic moderate-to-strong oceanic turbulence channels with the Málaga fading model. *Opt. Express* **2020**, *28*, 24056–24068. [CrossRef] [PubMed]
25. Lin, Z.; Xu, G.; Zhang, Q.; Somg, Z. Average symbol error probability and channel capacity of the underwater wireless optical communication systems over oceanic turbulence with pointing error impairments. *Opt. Express* **2022**, *30*, 15327–15343. [CrossRef] [PubMed]
26. Zhang, Y.; Zheng, Y.; Yan, Q.; Yu, L. Average capacity of an absorptive turbulent ocean channel with diffraction-and attenuation-resistant beam carriers. *Opt. Commun.* **2021**, *499*, 127291. [CrossRef]
27. Matta, G.; Pandey, P.; Agrawal, M.; Bahl, R. Capacity analysis of underwater visible light communication systems over a lossy channel in the presence of noises. *J. Opt. Soc. Am. A* **2022**, *39*, 948–958. [CrossRef]
28. Chauhan, D.S.; Kaur, G.; Kumar, D. Design of novel MIMO UOWC link using gamma–gamma fading channel for IoUTs. *Opt. Quantum Electron.* **2022**, *54*, 512. [CrossRef]

29. Wang, W.; Wang, P.; Pang, W.; Pan, Y.; Nie, Y.; Guo, L. Evolution properties and spatial-mode UWOC performances of the perfect vortex beam subject to oceanic turbulence. *IEEE Trans. Commun.* **2021**, *69*, 7647–7658. [CrossRef]
30. Li, Y.; Cui, Z.; Han, Y.; Hui, Y. Channel capacity of orbital-angular-momentumbased wireless communication systems with partially coherent elegant Laguerre–Gaussian beams in oceanic turbulence. *J. Opt. Soc. Am. A* **2019**, *36*, 471–477. [CrossRef]
31. Andrews, L.C.; Phillips, R.L. *Laser Beam Propagation through Random Media*, 2nd ed.; SPIE: Bellingham, WA, USA, 2005.
32. Jeffrey, A.; Zwillinger, D. *Table of Integrals, Series, and Products*; Academic Press: Cambridge, MA, USA, 2007.
33. Farid, A.A.; Hranilovic, S. Outage capacity optimization for free-space optical links with pointing errors. *J. Light. Technol.* **2007**, *25*, 1702–1710. [CrossRef]
34. Djordjevic, I.B.; Arabaci, M. LDPC-coded orbital angular momentum (OAM) modulation for free-space optical communication. *Opt. Express* **2010**, *18*, 24722–24728. [CrossRef]
35. Fewell, M.P.; Trojan, A.V. Absorption of light by water in the region of high transparency: Recommended values for photon-transport calculations. *Appl. Opt.* **2019**, *58*, 2408–2421. [CrossRef]